Photocurrent quantum yield of semiconducting carbon nanotubes: Dependence on excitation energy and exciton binding energy

Said Kazaoui,[1] Steffan Cook,[1] Nicolas Izard,[2] Yoichi Murakami,[3] Shigeo Maruyama [4] and Nobutsugu Minami[1]*

[1] National Institute of Advance Industrial Science and Technology (AIST), Japan

[2] Institut d'Electronique Fondamentale, Universite Paris-Sud, France

[3] Global Edge Institute, Tokyo Institute of Technology, Japan

[4] Department of Mechanical Engineering, The University of Tokyo, Japan

KEYWORDS: carbon nanotubes, semiconducting, photocurrent, optical absorption, quantum yield, exciton, binding energy

ABSTRACT: We address the dependence of the relative photocurrent quantum yield (QY) on the excitation energy and the exciton binding energy of semiconducting single wall carbon nanotubes (s-SWNTs) having well-defined chiral indexes, by analyzing both the optical absorption and the photocurrent spectra. First, we examine the QY of a sample consisting of a one sort of nanotube (such as (7,5)), which allows to reveal that QY depends on the excitation energy and hence on the nature of the electronic transition. In particular, we demonstrate that although the excitonic transitions dominate the OA and PC spectra, their quantum yields are relatively low compared with the band-to-band transitions. Then, we extend the analysis to a sample consisting of five kinds of nanotubes (namely (7,5), (7,6), (8,6), (8,7), (9,7)), which permits to demonstrate for the first time that QY increases with increasing the nanotube's diameter and with decreasing the exciton binding energy, according to two categories known as type 1 and type 2 nanotubes. Finally, we discuss these results in the framework of the electric field assisted exciton dissociation model in order to gain further insight into the photocarrier generation mechanism in s-SWNTs.

1. INTRODUCTION

Semiconducting single wall carbon nanotubes (s-SWNTs) are interesting one-dimensional nano-materials, which exhibit various optoelectronic properties such as electroluminescence and photoconductivity.[1] Several basic features of the photoconductivity such as spectral response, photocarrier generation and quantum yield were investigated using either ensemble or single s-SWNTs.[2,3,4,5,6] Very recently, the photocurrent quantum yield of suspended s-SWNTs in the split-gate field effect transistor configuration was reported by Malapanis.[6] However, the dependence of photocurrent quantum yield on the excitation energy and the exciton binding energy are still unexplored, despite the fact that such important information are expected to shed light onto the photocarrier generation mechanism in s-SWNTs.

In the present study, we undertake an unprecedented approach to address the relative quantum yield (QY) of s-SWNTs having well-defined chiral indexes by analyzing both the experimental optical absorption (OA) and photocurrent (PC) spectra. It should be stressed that the availability of macroscopic quantities of well-defined s-SWNTs permits the use of a wide range of conventional optical spectroscopy such as OA and PC, as described in the "Experimental Section". Applying these techniques to a sample consisting of one sort of nanotubes (such as (7,5)), allows to address the dependence of QY on excitation energy and on the nature of the excited state. Then, by extending this analysis to a bulk sample consisting of five kinds of nanotubes (such as (7,5), (7,6), (8,6), (8,7), (9,7)), we explore the dependence of QY on the diameter (d), the exciton transition energy (E_{11}) and the exciton binding energy (E_{b11}) of the first excitonic transition, as described in the section "Results and Discussion". Finally, these data are analyzed in the framework of the electric field assisted exciton dissociation model,[7] in order to gain new insight into the photocarrier generation mechanism in s-SWNTs.

2. EXPERIMENTAL SECTION

Semiconducting nanotubes with well-defined chiral indexes were selectively extracted from carbon nanotubes powders (such as Hipco and CoMoCat) using PFO (poly-9,9-di-n-octylfluorenyl-2,7-diyl) as an extracting agent in toluene solution prepared by ultrasonication and ultracentrifugation techniques.[8,9,10] These samples contain s-SWNTs free from metallic nanotubes, catalysts and graphitic impurities but contain traces of PFO, as confirmed by transmission electron microscopy, optical spectroscopy and electrical measurements. We prepared several kinds of samples consisting of either one sort of nanotubes (such as (7,5) or (8,7)) or an ensemble of nanotubes (such as (7,5), (7,6), (8,6), (8,7), (9,7)). The chiral indexes (n,m) were determined by mapping the photoluminescence emission spectra at several excitation wavelengths using a Fluorolog-3 spectrofluorometer (Supporting Information SI-1). Note that (7,5), (8,6) and (9,7) are categorized as type 1, while (7,6) and (8,7) are categorized as type 2, according to the definition (2n+m)mod3 equal 1 or 2 (with n and m integers).[11,12]

The s-SWNTs solutions were coated either on bare quartz substrates for OA measurements or on quartz substrates pre-patterned with interdigitated Au/Cr electrodes (100μm gap) for PC measurements. The OA spectra were recorded in the transmission mode with a Shimadzu UV-3600 spectrophotometer. The photocurrent intensity, defined as $I_{ph}=I_{light}-I_{dark}$ at a constant voltage and excitation wavelength, was measured using a lock-in amplifier with light modulated at 3Hz (I_{light} and I_{dark} are the current with and without light, respectively). The PC spectra were obtained by recording I_{ph} at a constant voltage while scanning the excitation wavelength, and were subsequently corrected for a constant photon flux.

From the experimental PC and OA spectra of s-SWNTs, we have calculated the relative photocurrent quantum yield (QY) defined as the number of photogenerated and collected charges per absorbed photon in the device. Here, we assume that the number of absorbed photons is approximately proportional to the absorbance of sample measured by OA spectroscopy for small absorbances (typically lower than 0.1). For the most resolved features observed in the PC and OA spectra, we have explicitly calculated QY by dividing the integrated area under the PC peak by the integrated area under the corresponding OA peak. The peak areas were calculated by fitting the entire OA and PC spectra with a sum-of-Gaussian function including a background. Note that OA and PC are in arbitrary units, and therefore QY are relative values.

3. RESULTS AND DISCUSSION

3.1. Excitation energy dependence of QY.

To address the excitation energy dependence of QY, we have analyzed the PC and OA spectra of (7,5) nanotube, as presented in figure 1 (a).

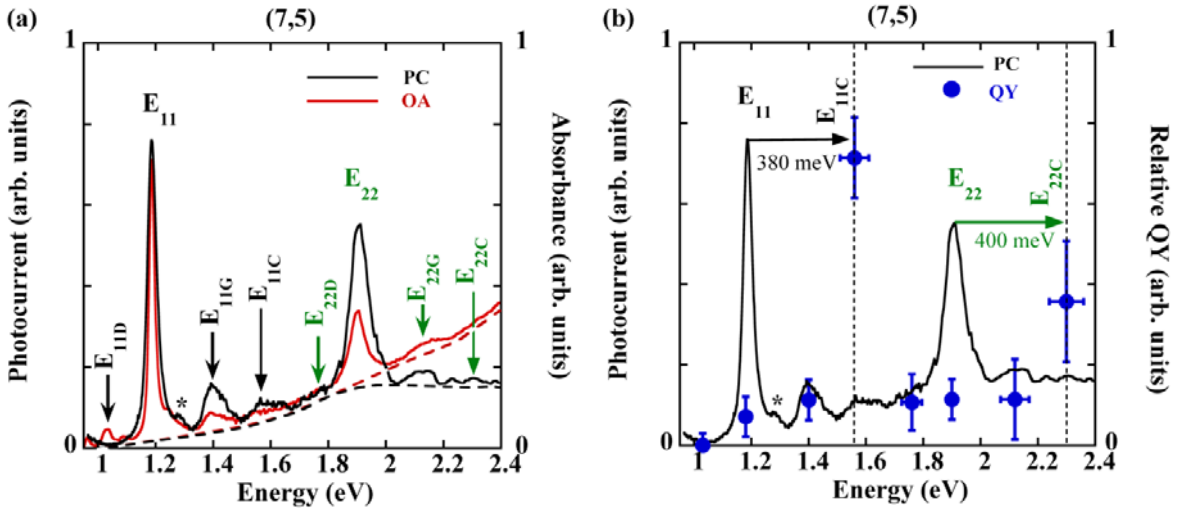

Fig.1 (online color only): (a) OA and PC spectra of (7,5) nanotube. The PC spectrum is recorded at an electric field of 2V/μm at room temperature. The backgrounds are indicated with dotted-lines (guide-to-the-eyes). (b) The relative photocurrent quantum yield (QY) and the PC spectrum. The labels are explained in the main text, the unassigned peak are labeled with *, and the uncertainty related to QY are indicated with error-bars.

The sharpest peak at 1.18eV (labeled E_{11}), which is observed in both the experimental PC and OA spectra, is assigned to the first optically allowed excitonic transition. This peak is accompanied by 2 satellite peaks at 1.40 eV (E_{11G}) and at 1.02 eV (E_{11D}), which are 220 meV above and 160 meV below E_{11}, respectively. These features are due to a strong coupling between a dipole-forbidden exciton and a K-point transverse optical phonon according to the literature.[9] The feature at 1.56 eV (labeled E_{11C}), which is resolved in the PC spectra but relatively weak in the OA spectra, is assigned to the band-to-band transition (Supporting Information SI-2). The second sharpest peak at 1.90 eV (labeled E_{22}), which is observed in both the OA and PC spectra,

is assigned to the second optically allowed excitonic transition. The E_{22G} and E_{22D} satellite peaks, observed at 220 meV above and 140 meV below E_{22} peak, are assigned to phonon-assisted transitions by analogy with our previous discussions. The feature at approximately 2.30 eV (labeled E_{22C}) is assigned to the second continuum level (this feature is poorly resolved in the PC spectrum at room temperature but relatively more resolved at 77K (Supporting Information SI-2)). The assignments of the PC and OA spectra of (7,5) nanotube are consistent with the previous studies, [1,5,13] although in the latter the chiral indexes of the s-SWNTs were unspecified.

The above-mentioned features are superimposed on broad backgrounds, which are shown with doted-lines in OA and PC spectra (Fig. 1(a)), but the origin and the shape of these backgrounds are not yet fully understood. Regarding the OA spectrum, the background might be due to light scattering and/or to the tail of the π-plasmon absorption.[14] The background underneath the PC spectrum is probably due to the continuum levels and its tail. These backgrounds are taking into account to fit the PC and OA spectra with a sum-of-Gaussian function, and to calculate the peak areas and QY.

In figure 1(b), we have plotted the relative QY together with the PC spectra. In the range of the E_{11} feature, we observed that QY increases with increasing the excitation energy in the following sequence: $QY(E_{11D})\sim0$, $QY(E_{11})=0.07$, $QY(E_{11G})=0.11$ and then sharply increases to $QY(E_{11C})\sim0.71$. At higher energy, in the range of the E_{22} peak, QY is almost constant with $QY(E_{22D})$ and $QY(E_{22})$ ~0.1 and then increases to $QY(E_{11C})\sim0.35$. Note that $QY(E_{11C})$ and $QY(E_{22C})$ are approximately 10 and 5 times larger than $QY(E_{11})$, respectively. In light of these results, we would like to emphasize that the photocurrent response predominantly originates

from the excitonic transitions (E_{11}, E_{22}), but their quantum yields are relatively low compared with the band-to-band transitions (E_{11C}, E_{22C}). It is also worth noticing that the high-order excitonic transitions (such as E_{22}) and the phonon-assisted transitions (such as E_{11G}) exhibit relatively higher quantum yields than that of E_{11}. This result is probably due to auto-ionization and phonon-assisted exciton ionization mechanisms, which were suggested by Perebeinos et al.[1,7]

A corollary of this assignment is that the exciton binding energy of E_{11} and E_{22} states of (7,5) are $E_{b11}=E_{11}-E_{11C}$=380 meV and $E_{b22}=E_{22}-E_{22C}$=400 meV, respectively. Such relatively large binding energy is one piece of evidence that explains the lower quantum yields of excitonic transitions (E_{11}, E_{22}) compared with band-to-band transitions (E_{11C}, E_{22C}). It is worth mentioning that E_{b11} deduced from PC spectroscopy is in agreement with that deduced from the 2-photon photoluminescence excitation spectroscopy (E_{b11}=390 meV).[15]

Similar conclusions were reached from the analysis of OA and PC spectra of (8,7) nanotube. A remarkable difference is that the binding energy of the E_{11} state in (8,7) nanotube is E_{b11}=310 meV, which is relatively lower than that of the corresponding transition in (7,5) nanotube (Supporting Information SI-3). Regarding the relative QY of (8,7) compared with (7,5) nanotube, we were unable to access it precisely because those two samples were measured under slightly different conditions. Taking a different approach, to be described in the following section, we shall systematically compare the QY of various s-SWNTs.

3.2. Dependence of QY on the chiral index, d, E_{11}, E_{b11} and nanotube type.

To explore the dependence of QY on the chiral index, d, E_{11}, E_{b11} and nanotube type, we have analyzed the PC and the OA spectra of a sample composed of an ensemble of (7,5), (7,6), (8,6), (8,7) and (9,7) nanotubes, as presented in the figure 2.

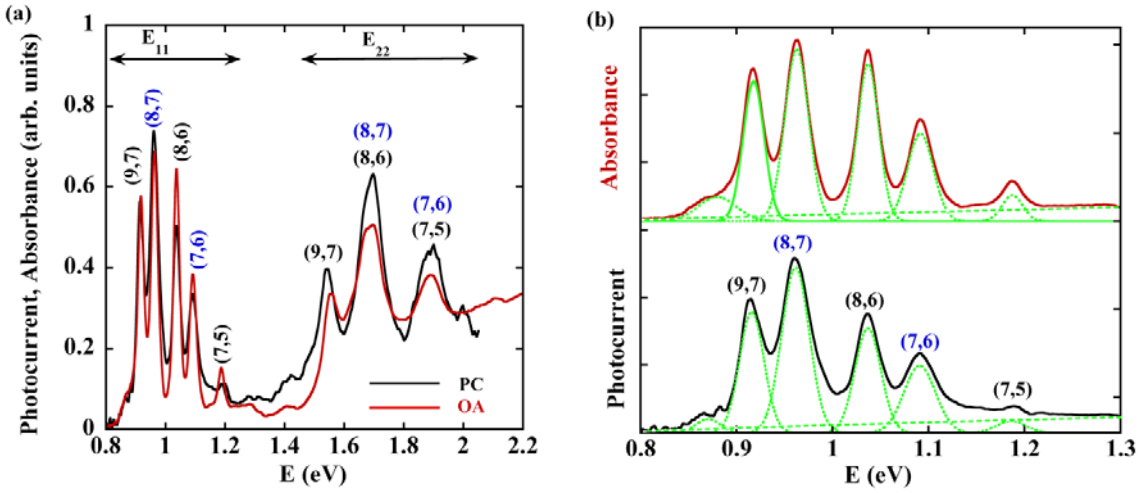

Fig.2 (online color only): (a) OA and PC spectra of an ensemble (n,m) s-SWNTs. The PC spectrum was recorded at an electric field of 1V/μm at room temperature. (b) OA and PC spectra are fitted with a sum-of-Gaussian function including a small background (shown with dotted line).

Despite the poly-dispersity of this sample, the PC and OA spectra exhibit very well-resolved peaks in the low-energy range corresponding to E_{11} excited states of various (n,m) nanotubes. In contrast, the higher-order excited states (such as E_{11D}, E_{11G}, E_{11C}, E_{22}) are spectrally unresolved. Therefore, in the forthcoming analysis, we shall focus on the low energy range (0.8~1.3 eV), as displayed in figure 2(b). The PC and OA spectra were fitted with a sum-of-Gaussian functions including a small background, as shown in figure 2(b), from which we have subsequently

calculated the peak areas and QY(E_{11}) for various nanotubes. Here, note that the backgrounds, shown with dotted-lines in figure 2(b), mainly originate from the overlap of several weak transitions (such as E_{11D}, E_{11G}, E_{11C}) due to various (n,m) s-SWNTs. The calculated QY(E_{11}) versus d, E_{11} and E_{b11} of various s-SWNTS are displayed in figures 3 and 4 (Note that similar results are obtained at various electric field, albeit some interesting differences to be reported elsewhere).

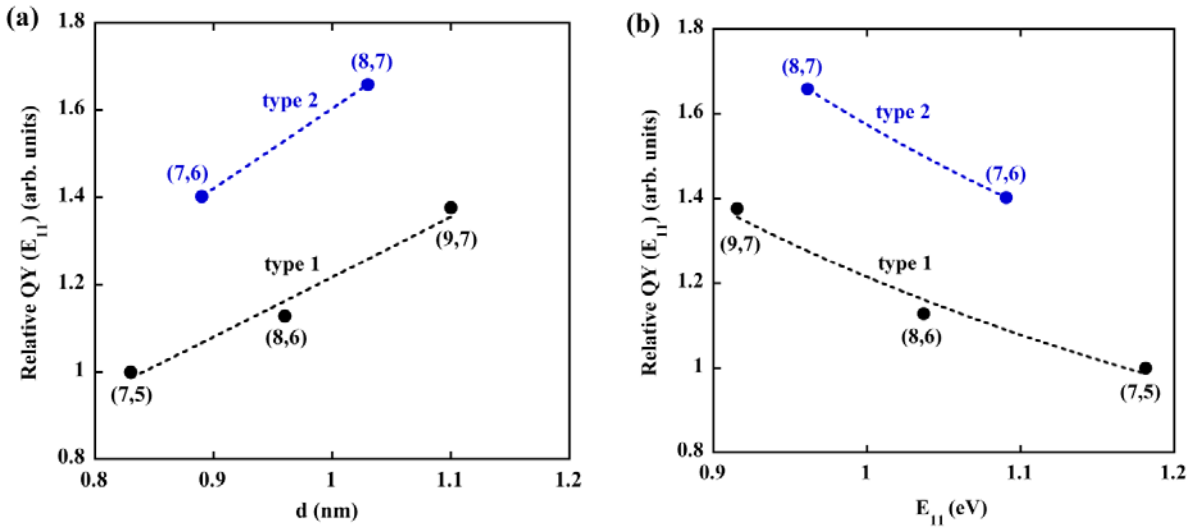

Fig. 3 (online color only): (a) and (b) display the relative QY(E_{11}) versus d and E_{11} for various (n,m) s-SWNTs, respectively. QY(E_{11}) are relative values, which are normalized to that of the (7,5) nanotube. Dotted-lines are guide-to-the-eyes.

Figures 3(a) and 3(b) unveil for the first time that QY(E_{11}) increases with increasing d and with decreasing E_{11}, respectively. Here, d are theoretical values, whereas E_{11} are the experimental values deduced from the PC spectra. A detailed analysis reveals that QY(E_{11}) versus either d or E_{11} can be divided into two categories highlighted with dotted-lines, which are known as type 1 and type 2 nanotubes. A quantitative analysis shows that QY(E11) scales as $(d)^{1.15}$ and $(d)^{1.13}$ for

type 1 and 2, respectively. We also observed that QY(E11) scales as $(E11)^{-1.33}$ and $(E11)^{-1.25}$ for type 1 and 2, respectively. It is remarkable that QY(E_{11}) for type 1 and type 2 follows two different but almost parallel trends.

Next, we shall examine the E_{b11} dependence of QY(E_{11}), because E_{b11} a crucial parameter that governs the dissociation of excitons. E_{b11} of (7,5) and (8,7) nanotubes are determined by PC spectroscopy, but those of (7,6), (8,6) and (9,7) are not yet obtained, because we were unable to extract and purify those samples with our technique. Alternatively, we can refer to E_{b11} estimated from 2-photon photoluminescence spectroscopy (2-photon PL).[15] This choice is motivated by the fact that for either (7,5) or (8,7), E_{b11} measured by PC (labeled with the symbol (●)) and 2-photon PL (labeled with the symbol (+)) are very similar, as shown in figure 4(a). The difference is probably due to the experimental conditions and the analytical methods that were used in the PC and the 2-photon PL experiments. It is worth noticing that E_{b11} exhibits the diameter and the nanotube type dependences (Fig. 4(a)), which are qualitatively consistent with the theoretical studies.[11,12] Taking into account E_{b11} measured by PC and 2-photon PL, we have revealed that QY(E_{11}) decreases with increasing E_{b11} according to type 1 and 2 behaviors, as presented in figure 4(b). According to the literatures, the properties of the exciton in s-SWNTs (such as transition energy, binding energy, effective mass and oscillator strength) are strongly affected by trigonal warping, curvature and lattice distortion effects.[11,12,16] By analogy, we think that these effects are the cause of the chiral index and type dependence of QY(E_{11}).

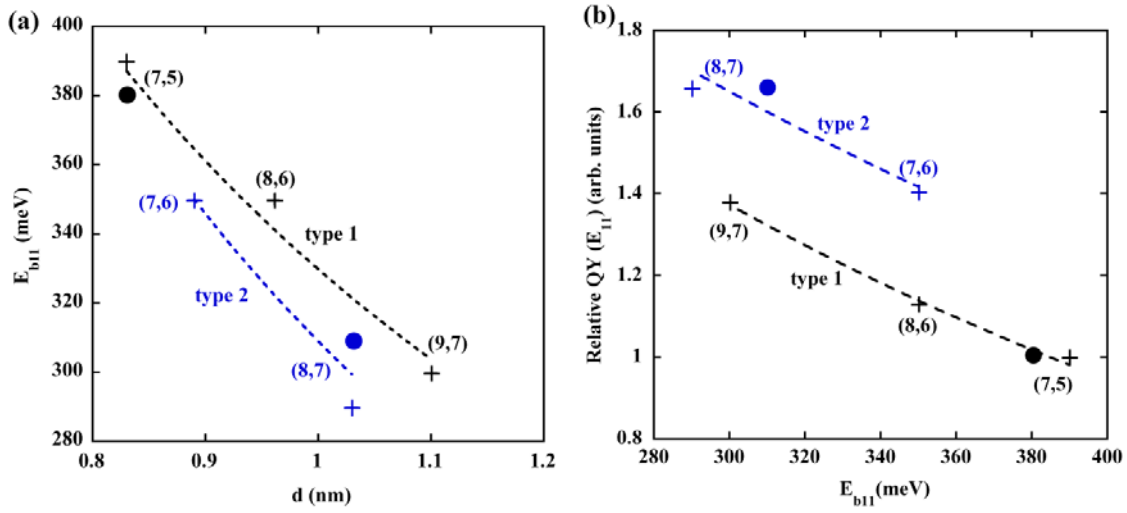

Fig. 4 (online color only): (a) E_{b11} versus diameter (d) for several (n,m) s-SWNTs. E_{b11} are from the PC data (labeled with the symbol (●)) and from the 2-photon data (labeled with the symbol (+)). (b) QY(E11) versus E_{b11} for several (n,m) s-SWNTs. QY(E_{11}) are relative values, which are normalized to that of the (7,5) nanotube. Dotted-lines are guide-to-the-eyes.

3.3. Analysis of the E_{b11} and the nanotube type dependence of QY(E_{11}).

To gain further knowledge, E_{b11} and the nanotube type dependence of QY(E_{11}) are qualitatively analyzed in the framework of the electric field assisted tunneling model for the dissociation of exciton in s-SWNTs.[1,7] In this model, the electric field assisted exciton dissociation rate Γ_0 is given by equation 1, where m_{11}^* is the reduced mass of the E_{11} exciton, F the electric field, e the charge of the electron, $\hbar$ the Planck constant , α and β constants.[1,7]

$$\Gamma_0 = \alpha E_{b11}\left(\frac{F_0}{F}\right)\exp\left(-\frac{F_0}{F}\right) \quad \text{with} \quad F_0 = \beta E_{b11}^{3/2} m_{11}^{*1/2}/e\hbar \qquad (1)$$

Furthermore, we assume QY(E_{11})~Γ_0, because we are only interested in the relative difference in the carrier generation step among different s-SWNTs. In addition, we are intentionally

discarding the term related to carrier transport through the random network of the nanotubes, because the mobility of the carrier in such a system is inevitably averaged and expected to lose systematic dependence on the chiral indexes.

Equation 1, which is governed by the exponential term in the low electric field regime ($e\hbar F << E_{b11}$), predicts that $QY(E_{11})$ decreases with increasing E_{b11} for either type 1 or 2 nanotube (at constant F). Indeed, as shown in figure 4(b), $QY(E_{11})$ qualitatively scales as $4.1\exp(-0.0030E_{b11})$ and $4.2\exp(-0.0037E_{b11})$ for type 1 or 2 nanotube, respectively. One should take these scaling relations as guide line but not literally, because the number of points and the energy range are rather limited. Equation 1 also permits to rationalize the nanotube type dependence of $QY(E_{11})$, by recognizing that type 1 compared with type 2 nanotubes are theoretically characterized by a relatively higher m_{11}^*.[11] In this context, if m_{11}^* of type 1 is higher than that of type 2 nanotube, then type 1 should exhibits lower Γ_0 and QY than type 2 nanotube (at constant E_{b11}, F). Indeed, we have experimentally observed that QY of (8,6) nanotube (type 1) is lower than that of (7,6) nanotube (type 2), although these two sorts of nanotubes are characterized by a very similar binding energy. In substance, this simple analysis allows to account for the E_{b11} and the nanotube type dependence of $QY(E_{11})$, which suggests that a strongly bound E_{11} exciton in s-SWNTS can dissociate by the electric field assisted tunneling mechanism. Admittedly, to validate this model and explore others,[17,18,19] a comprehensive study of the electric field dependence of $QY(E_{11})$ must be performed in the future.

4. CONCLUSIONS

In conclusion, by performing a systematic analysis of the PC and OA spectra of well-defined s-SWNTs consisting of either one sort of nanotube (such as (7,5)) or a limited sort of nanotubes (such as (7,5), (7,6), (8,6), (8,7) and (9,7)), we have experimentally demonstrated that the relative QY depends on the excitation energy and on the nature of the excited state. In particular, we have demonstrated that although the excitonic transitions (E_{11}, E_{22}) dominate the photocurrent spectrum, their quantum yields are relatively low compared with the band-to-band transitions (E_{11C}, E_{22C}). In addition, we have shown that $QY(E_{22})>QY(E_{11})$, which is probably due to auto-ionization and phonon-assisted exciton ionization mechanisms. We have also demonstrated for the first time that $QY(E_{11})$ increases with increasing d, decreasing E_{11} and decreasing E_{b11} according to two categories known as type 1 and type 2 nanotubes. In particular, we have observed that $QY(E_{11})$ of type 1 is lower than that of type 2, because according to theoretical studies the reduced exciton mass (m_{11}^*) of the former is larger than that of the latter. Finally, we have shown that the E_{b11} and nanotube type dependence of $QY(E_{11})$ can be qualitatively rationalized in the framework of the electric field assisted tunneling model for the dissociation of exciton in s-SWNTs. We hope that the present results will trigger further experimental and theoretical studies to elucidate the photocarrier generation mechanism in one-dimentional s-SWNTs. We also expect that the present study will contribute to the development of s-SWNTs based photodetectors and photovoltaics.

ASSOCIATED CONTENT

Supporting Information. Identification of the chiral indexes of the nanotubes (Supporting Information SI-1), Electric field and temperature dependence of the PC spectra (Supporting Information SI-2), PC and OA spectra of (8,7) compared with (7,5) nanotubes (Supporting Information SI-3). This material is available free of charge via the Internet at http://pubs.acs.org.

AUTHOR INFORMATION

* Kazaoui Said e-mail: s-kazaoui@aist.go.jp

REFERENCES

(1) Avouris, P.; Freitag, M.; Perebeinos, V. In *CARBON NANOTUBES: ADVANCED TOPICS IN THE SYNTHESIS, STRUCTURE, PROPERTIES AND APPLICATIONS*; 2008; Vol. 111, pp. 423–454.

(2) Fujiwara, A.; Matsuoka, Y.; Suematsu, H.; Ogawa, N.; Miyano, K.; Kataura, H.; Maniwa, Y.; Suzuki, S.; Achiba, Y. *Jpn. J. Appl. Phys. Part 2-LETTERS* **2001**, *40*.

(3) Beard, M. C.; Blackburn, J. L.; Heben, M. J. *Nano Lett.* **2008**, *8*, 4238–4242.

(4) Freitag, M.; Martin, Y.; Misewich, J. A.; Martel, R.; Avouris, P. *Nano Lett.* **2003**, *3*, 1067–1071.

(5) Mohite, A.; Lin, J.-T.; Sumanasekera, G.; Alphenaar, B. W. *Nano Lett.* **2006**, *6*, 1369–1373.

(6) Malapanis, A.; Perebeinos, V.; Sinha, D. P.; Comfort, E.; Lee, J. U. *Nano Lett.* **2013**, *13*, 3531–3538.

(7) Perebeinos, V.; Avouris, P. *Nano Lett.* **2007**, *7*, 609–613.

(8) Izard, N.; Kazaoui, S.; Hata, K.; Okazaki, T.; Saito, T.; Iijima, S.; Minami, N. *Appl. Phys. Lett.* **2008**, *92*.

(9) Murakami, Y.; Lu, B.; Kazaoui, S.; Minami, N.; Okubo, T.; Maruyama, S. *Phys. Rev. B* **2009**, *79*.

(10) Nish, A.; Hwang, J.-Y.; Doig, J.; Nicholas, R. J. *Nat Nano* **2007**, *2*, 640–646.

(11) Jiang, J.; Saito, R.; Samsonidze, G. G.; Jorio, A.; Chou, S. G.; Dresselhaus, G.; Dresselhaus, M. S. *Phys. Rev. B* **2007**, *75*.

(12) Capaz, R. B.; Spataru, C. D.; Ismail-Beigi, S.; Louie, S. G. *Phys. Rev. B* **2006**, *74*.

(13) Mohite, A. D.; Gopinath, P.; Shah, H. M.; Alphenaar, B. W. *Nano Lett.* **2007**, *8*, 142–146.

(14) Kataura, H.; Kumazawa, Y.; Maniwa, Y.; Umezu, I.; Suzuki, S.; Ohtsuka, Y.; Achiba, Y. *Synth. Met.* **1999**, *103*, 2555–2558.

(15) Dukovic, G.; Wang, F.; Song, D.; Sfeir, M. Y.; Heinz, T. F.; Brus, L. E. *Nano Lett.* **2005**, *5*, 2314–2318.

(16) Ando, T. *J. Phys. Soc. Jpn.* **2009**, *78*.

(17) Emelianova, E. V.; Auweraer, M. van der; Bassler, H. *J. Chem. Phys.* **2008**, *128*.

(18) Moses, D.; Wang, J.; Heeger, A. J.; Kirova, N.; Brazovski, S. *Proc. Natl. Acad. Sci. United STATES Am.* **2001**, *98*, 13496–13500.

(19) Konabe, S.; Okada, S. *Appl. Phys. Lett.* **2013**, *102*, 113110.

Supporting Information

Photocurrent Quantum Yield of Semiconducting Carbon Nanotubes: Dependence on Excitation Energy and Exciton Binding Energy

Said Kazaoui,[1] Steffan Cook,[1] Nicolas Izard,[2] Yoichi Murakami,[3] Shigeo Maruyama [4] and Nobutsugu Minami[1]*

[1] National Institute of Advance Industrial Science and Technology (AIST), Japan

[2] Institut d'Electronique Fondamentale, CNRS-UMR 8622, Universite Paris-Sud, France

[3] Department of Mechanical Sciences and Engineering,Tokyo Institute of Technology, Japan

[4] Department of Mechanical Engineering, The University of Tokyo, Japan

Supporting Information 1 (SI-1): Identification of the chiral indexes of the nanotubes.

The chiral indexes of the nanotubes were determined by mapping the photoluminescence emission spectra at several excitation wavelengths using a Fluorolog-3 spectrofluorometer. We found that the samples consist of either one sort of nanotubes (such as (7,5)) or limited number of nanotubes (such as (7,5), (7,6), (8,6), (8,7) and (9,7)).

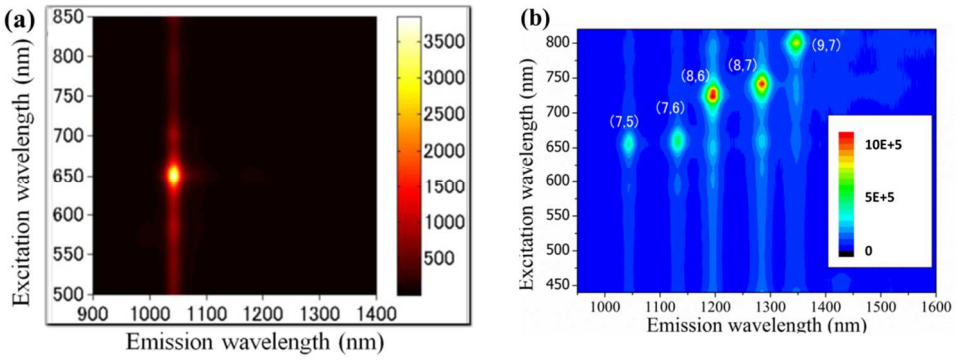

Figure SI-1: Photoluminescence excitation maps of a bulk sample consisting of only (7,5) and a bulk sample consisting of five kinds of nanotubes (namely (7,5), (7,6), (8,6), (8,7), (9,7)) are presented in (a) and (b), respectively .

Supporting Information 2 (SI-2): Photocurrent measurements

Figure SI-2-1(a) displays the configuration of our pre-patterned interdigitated Au electrodes (100mm gap) on quartz substrates. SWNTs are subsequently deposited on top of these electrodes. The electric field is applied in the plane between the Au electrodes, as shown with the arrow, and the incident light is perpendicular to this direction. Figure SI-2-1(b) presents the Atomic Force Microscope image (AFM, Topography) of our bulk nanotube sample, which forms a network of nanotubes. The thicknesses of the samples utilized for PC are thinner than used for OA measurements, but both are unfortunately unknown.

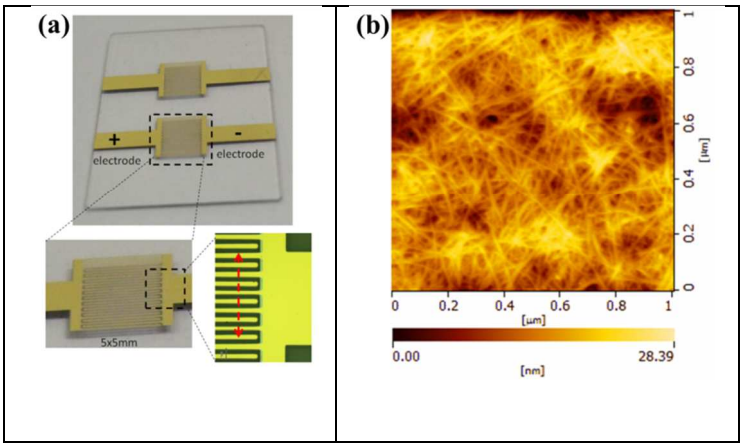

Figure SI-2-1: (a) displays the configuration of the electrodes typically used in our PC experiment (without nanotubes); (b) presents a typical AFM image (topography) of our nanotube sample.

The raw photocurrent signal (I_{ph}), defined as $I_{ph}=I_{light}-I_{dark}$ at a constant voltage and excitation energy (E_{ex}), was measured using a lock-in amplifier with light modulated at 3Hz (I_{light} and I_{dark} are the current with and without light, respectively). The PC spectra were obtained by recording I_{ph} at a constant voltage while scanning the excitation energy (in fact, wavelength scan), as shown in figure SI-2-2(a). To cover the entire excitation energy range, we utilized a halogen lamp and a monochromator equipped with 2 gratings, which causes the discontinuity observed at around 2eV. To obtain the photocurrent spectrum at constant photon flux, we measured the spectral response of the halogen lamp, as shown in figure SI-2-2(a), using a pyro-detector and the same monochromator equipped with the same gratings. Then, the lamp's incident power density (P_{in}) was converted to the incident photons flux (N_{in}) at every E_{ex}, as shown in figure SI-2-2(b), using the following relatsion (with q=1.6x10^{-19}):

$$N_{in}[\text{photon s}^{-1}\ \text{m}^{-2}]=P_{in}[\text{W m}^{-2}]/(qE_{ex}[\text{eV}])=6.25*10^{+18}P_{in}[\text{W m}^{-2}]/(E_{ex}[\text{eV}])$$

Finally, the raw photocurrent signal (I_{ph}) was divided by the number of incident photons (N_{in}) at every E_{ex}, in order to obtain the photocurrent spectra normalized to the incident photon flux, as displayed in the figure SI-2-2(c). The unit of the photocurrent normalized to the photons flux is (A/(photon s^{-1} m^{-2})), where the current is in ampere (A) and photon stand for the number of photon. For convenience, in the forthcoming analysis, the units of photocurrent normalized to the incident photon flux will be displayed in ampere (A) instead of A/(photon s^{-1} m^{-2}).

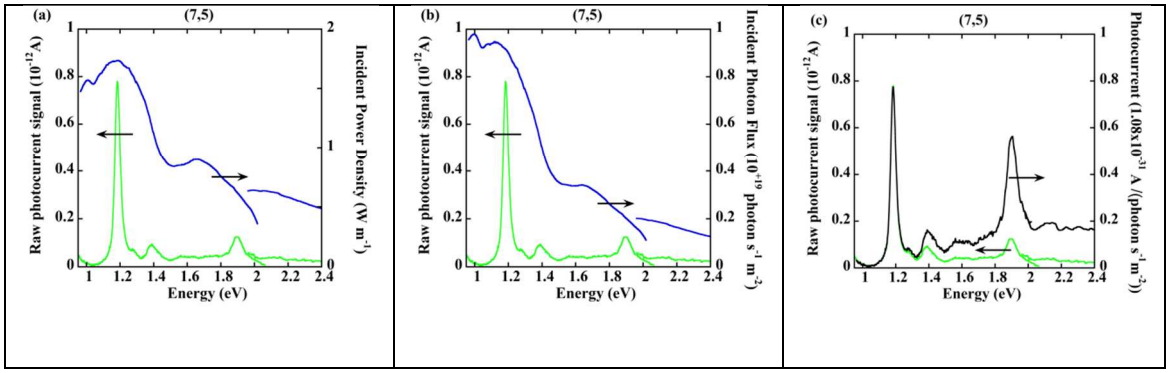

Figure SI-2-2: (a) and (b) present the PC spectra of (7,5) nanotube together with the spectral response of the lamp plus monochromator (incident power or number of incident photons). (c) shows the photocurrent spectra before and after normalization to a constant photon flux.

Supporting Information 3 (SI-3): QY calculations

Method 1: First, the backgrounds shown with dotted-lines are subtracted from the PC and OA spectra. Figure SI-3 (a), (b) and figure SI-3 (c), (d) are before and after background subtraction, respectively. Then, the entire PC and OA spectra are fitted with sum-of-Gaussian functions (Fig. SI-3 (e), (f)). Finally, QY is calculated by dividing the area or the amplitude of the Gaussian function of the each PC peak by that of corresponding OA peak. Here, we address the QY of E_{11}, E_{22} and E_{11G}, as summarized in Table 1, but we don't present the QY of E_{11C}, E_{22C}, E_{11D}, E_{22D} and E_{22G}, because the latter have large uncertainty.

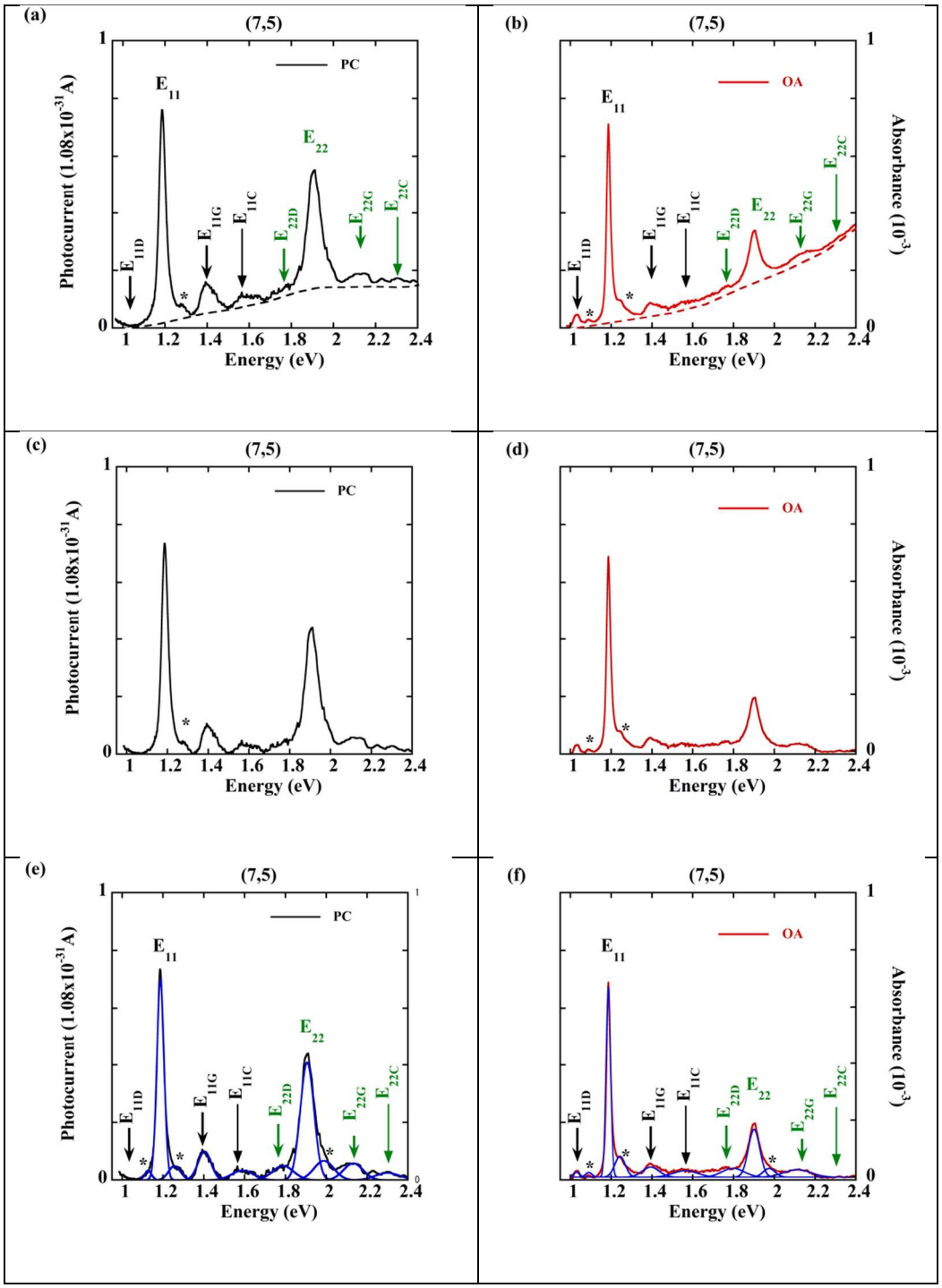

Figure SI-3-1: (a) and (b) present the PC and the OA spectra of (7,5); (c) and (d) those after background subtraction; (e) and (f) those after fitting the sum-of-Gaussian functions. Note that the PC and the OA spectra are arbitrarily scale to 1. The labels are explained in the main text, the unassigned features are labeled with *.

Table 1: Using Method 1 the QY of the E_{11}, E_{22} and E_{11G} were calculated. The table shows the photocurrent intensity (PC) in amperes divided $1.08x10^{-31}$, the Absorbance (OA) divided 10^{-3}, and QY in electron/photon divided by $6.75x10^{-10}$.

Method 1	PC peak area	OA peak area	QY=PC/OA area	PC peak amplitude	OA peak amplitude	QY=PC/OA amplitude
E_{11} peak	0.03082	0.014505	2.1247	0.70188	0.60815	1.1541
E_{11G} peak	0.00786	0.003597	2.1851	0.098989	0.035145	2.8166
E_{22} peak	0.03394	0.011628	2.9188	0.40899	0.16806	2.4336

QY is calculated using the relation: QY=Photocurrent (A)/(number of absorbed photons s^{-1}). Since we assume that number of absorbed photons per second is proportional to the absorbance, and since1A=1Coulomb s^{-1}=$6.25x10^{+18}$ electrons s^{-1}, then

$$QY=6.25x10^{+18}\ \text{Photocurrent (A)/(Absorbance) [electron/photon]}$$

The QY values reported in Table 1 and 2 are relative values and should not be taking literally. Although the calculated QY values are relatively different depending on the parameters of the Gaussian functions that were used to calculate the quantum yield QY (Table 1), we consistently observed that the high-order excitonic transitions (such as E_{22}) and the phonon-assisted transitions (such as E_{11G}) exhibit relatively higher quantum yields than that of E_{11}.

Method 2: The QYs were simply calculated from the PC and OA spectra taking into account the peak area (dashed area), the peak height (vertical arrow) and the total peak height from the zero level (vertical dashed arrow), as illustrated in figure SI-3-2. In contrast with Method 1, the PC and OA spectra are not fitted with sum-of-Gaussian functions.

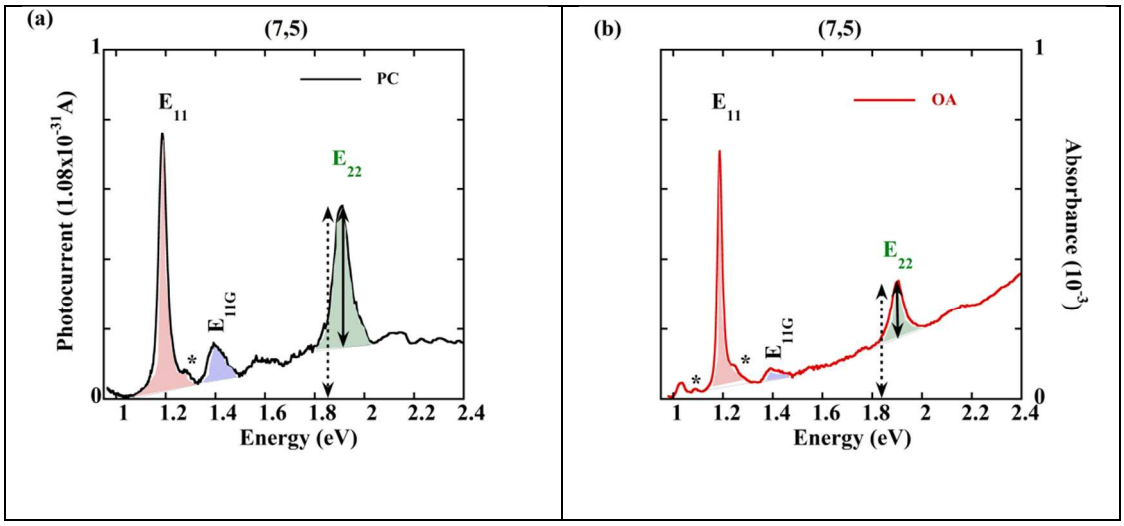

Figure SI-3-2: (a) and (b) present the PC and the OA spectra of (7,5). The peak area (dashed area) of the E_{11}, E_{22} and E_{11G} electronic transitions are shown. The meaning of the peak height (vertical arrow) and the total peak height (vertical dashed arrow) are shown on E_{22} peak.

Table 2: Using Method 2 the QY of the E_{11}, E_{22} and E_{11G} were calculated. The table shows the photocurrent intensity in amperes divided $1.08x10^{-31}$, the Absorbance divided 10^{-3}, QY in electron/photon divided by $6.75x10^{-10}$.

Method 2	PC peak area	OA peak area	QY=PC/OA area	QY Peak height	QY total peak height
E_{11} peak	0.03307	0.02104	1.5717	1.077	1.070
E_{11G} peak	0.03357	0.011089	3.0248	2.466	1.825
E_{22} peak	0.00735	0.002419	3.0384	2.980	1.622

Table 2 presents the QY calculated using the area, the peak height or the total peak height of the PC peak divided by that of the corresponding OA peak, as shown in figure SI-3-2. For the same reason mentioned earlier, the QY values of the E_{11}, E_{22} and E_{11G} should not be taking literally, and we don't present the QY of E_{11C}, E_{22C}, E_{11D}, E_{22D} and E_{22G} because their analysis results in large uncertainty. As summarized in figure SI-3-3, irrespective of the analytical method, we consistently observed that the high-order excitonic transitions (E_{22}) and the phonon-assisted transitions (E_{11G}) exhibit relatively higher quantum yields than that of E_{11}.

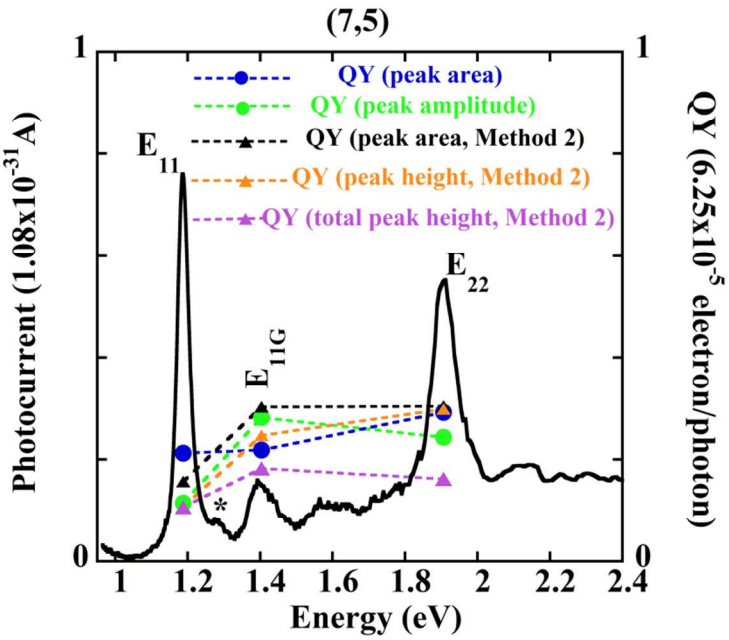

Figure SI-3-3: The figure presents the PC spectrum of (7,5) and the calculated QY of E_{11}, E_{22} and E_{11G} peak using different parameters and methods.

Supporting Information 4 (SI-4): Electric field dependence of the PC.

Figure SI-4 displays the electric field (F) dependence of the photocurrent peak intensity of various electronic transitions (E_{11}, E_{11G}, E_{22} and E_{11C} as already described). The features

observed in the PC spectra do not shift or broaden, but their intensities increase with increasing F. To gain further insight, we recoded the F dependence of the photocurrent peak intensity and we observed that the latter increases with increasing F according to a power-law (F^{α}), as presented in figure SI-4. We found that E_{11C} (which are characterized by α=1.49) exhibits a weak F dependence compared with E_{11}, E_{11G} and E_{22} (which are characterized by α=2.24, 1.98, 1.92, respectively). In addition, the F dependence of E_{11C} is relatively similar to that of the dark current (α=1.2), which means that the F dependence of E_{11C} mainly reflects the charge transport, trapping/detrapping and inter-tube hopping mechanisms of the photogenerated free electrons and holes. In contrast, the E_{11} and E_{22} excitons are strongly F dependent, because excitons inevitably require electric field to dissociate into free carriers. These results provide further support to our assignment that E_{11} and E_{22} are excitonic transitions, whereas E_{11C} is a band-to-band transition.

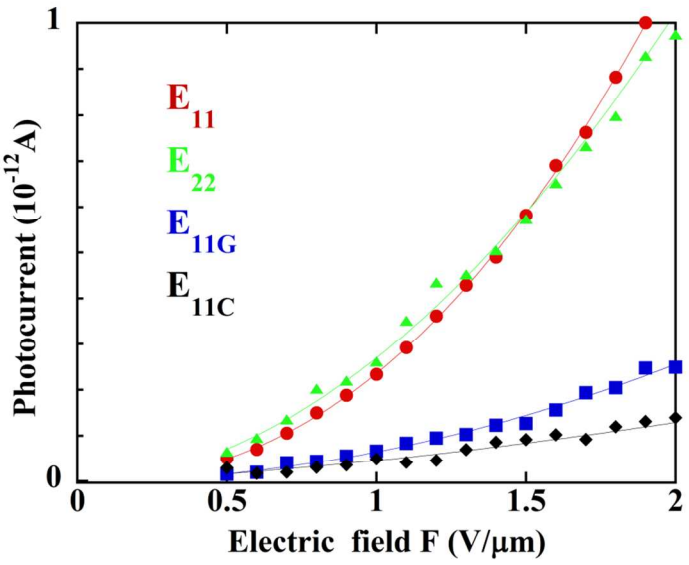

Figure SI-4: The photocurrent peak intensity of various electronic transitions (E_{11}, E_{11G}, E_{22} and E_{11C}) as functions of electric field (F).

Supporting Information 5 (SI-5): PC and OA spectra of (8,7) compared with (7,5) nanotubes. The (8,7) sample is obtained as follows. First, a sample consisting of five kinds of nanotubes ((7,5), (7,6), (8,6), (8,7), (9,7)) in PFO/toluene solution is mixed a P3HT/toluene solution (P3HT stands for poly(3-hexylthiophene-2,5-diyl)). After centrifugation of this mixture, we find that the supernatant solution contains (8,7) nanotubes, while the sediments contains all the other nanotubes. Subsequently, the supernatant solution was further centrifuged at very high speed in order to sediment and to collect the (8,7) nanotubes, which contains traces of PFO and P3HT. Figure SI-5(a) presents the PC and OA spectra of (8,7). The assignments of the OA and PC spectra of (8,7) are consistent with those reported for (7,5) nanotube, although the features are shifted to lower energy. The figure SI-5(b) presents the PC spectra of (8,7) and (7,5), which are shifted by ($-E_{11}$) and normalized at the E_{11} peaks to emphasize the relative position of the E_{11C} features. In particular, we found that the binding energies for the E_{11} excitonic transitions are E_{b11}=310 meV and E_{b11}=380 meV for (8,7) and (7,5) nanotubes, respectively.

To determine E_{b11}, we first identify the feature that corresponds to E_{11C}. Then, we can take the energy of either the onset or the maximum of E_{11C} feature. However, since there are features below E_{11C}, the onset is difficult to distinguish. Alternatively, we have decided to take the maximum of the E_{11C} feature, although the E_{11C} is relatively broad (which is the main source of error). Finally, E_{b11} is simply calculated as $E_{b11}=E_{11}-E_{11C}$.

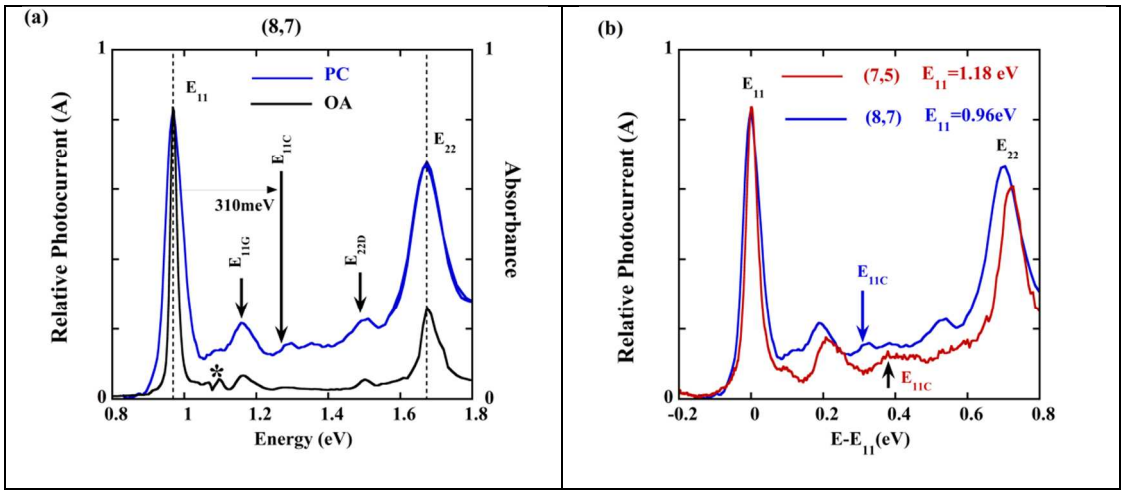

Figure SI-5: (a) PC and OA spectra of (8,7). (b) PC spectra of (8,7) and (7,5) shifted by ($-E_{11}$) and normalized at the E_{11} peaks.

Supporting Information 6 (SI-6): Dependence of QY on d and E_{11}.

To rationalize the dependence of QY on d and E_{11}, we have plotted E_{b11} as function d and E_{11}, as presented in figure SI-6(a) and (b).

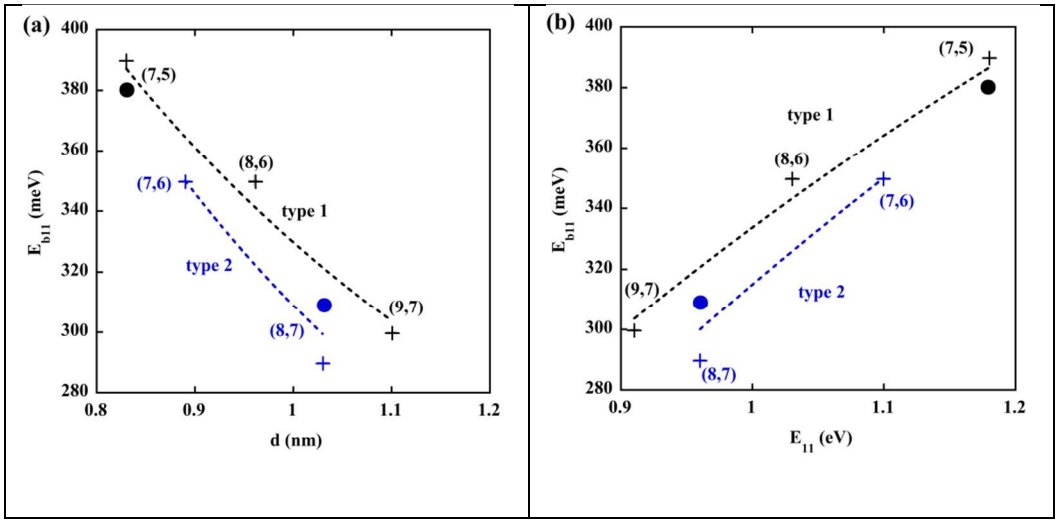

Figure SI-6: (a) and (b) display E_{b11} versus d and E_{11} for various (n,m) s-SWNTs, respectively. E_{b11} are from the PC data (labeled with the symbol (●)) and from the 2-photon data (labeled with the symbol (+)). Dotted-lines are guide-to-the-eyes.